Visual Abstract

Evaluation of the survivability of CFRP honeycomb-cored panels in compression after impact tests

Oleg A. Staroverov, Elena M. Strungar, Valery E. Wildemann
Perm National Research Polytechnic University, Russia
cem_staroverov@mail.ru, https://orcid.org/0000-0001-6095-0962
cem.spaskova@mail.ru, http://orcid.org/0000-0002-2246-8638
wildemann@pstu.ru, http: //orcid.org/0000-0002-6240-4022

ABSTRACT. This paper is oriented to the experimental research of the mechanics of the CFRP sandwich plates, glass and carbon fiber sample panels with a large-cell honeycomb core. The method for testing polymer composite sample plates in compression after impact (CAI) tests with joint use of a testing machine and a video system for deformation field registration was tested. Analysis of the experimental data obtained highlighted the impactive sensitivity zone for the test specimens. A quantitative assessment of the load-bearing capacity of glass and carbon fiber sample panels in CAI tests with the different levels of the drop weight impact energy was performed. Photos of samples after impact have been provided.
Vic-3D non-contact three-dimensional digital optical system was used to register the displacement and deformation fields on the surface of the samples. The video system was used to evaluate various damage mechanisms, including matrix cracking, delaminations, and rupture of the damaged fibers. The paper studied the evolution of non-homogeneous deformation fields on the surface of the composite samples during the post-impact compression tests and analyzed the configuration of non-homogeneous deformation fields.

KEYWORDS. Composite materials; Compression after impact; Digital image correlation; Stress concentrators; Residual strength; Life prediction.

OPEN ACCESS

Citation: Staroverov, O., A., Strungar, E, M., Wildemann, V, E. Evaluation of the survivability of CFRP honeycomb-cored panels in compression after impact tests, Frattura ed Integrità Strutturale, 56 (2021) 1-15.

Received: 10.09.2020
Accepted: 04.01.2021
Published: 01.04.2021

Copyright: © 2021 This is an open access article under the terms of the CC-BY 4.0, which permits unrestricted use, distribution, and reproduction in any medium, provided the original author and source are credited.

INTRODUCTION

The low-velocity impact is a serious threat to the use of composite materials in engineering applications, as they cause minute damages that can go unnoticed. The appearance of minute impact damage (BVID) in responsible composite components and structures is a serious problem that can lead to a reduction in the safety of aircraft or other equipment and must be replaced or repaired in a timely manner according to the safety requirements for the product.

The development of composite production technologies makes it possible to incorporate them into parts and components of critical structures, in particular in the aviation industry. Polymer matrix-based composites (PCM) are widely used due to their low cost of components and relatively high elastic behavior.

The hot topic of experimental mechanics is to obtain new experimental data on the processes of deformation and destruction of layered-fiber polymeric composite materials in the presence of operational stress concentrators. A large number of scientific papers [1-7] are devoted to the study of the residual strength degradation of composite sandwich plates under various environmental conditions. The paper describes the methods and progress of testing, the findings in the form of dependencies of the residual strength (maximum compressive load after impact) at the same level of impact (impact energy). However, there is no data on the changes in the residual properties when changing the parameters of the preliminary impact, in particular the potential impact energy. One of the important aspects of the materials research under the conditions of preliminary mechanical impacts is an identification of sensitivity threshold value [8,9]. This paper refers to the impactive sensitivity threshold, which is an energy value at which impacts with energies exceeding the threshold value lead to drastic changes in the residual mechanical properties of the material.

Apart from the tasks described above, the problems related to strain measurement under the combined stress caused by the presence of stress concentrators, as well as the analysis of fracture kinetics during the crack propagation while samples are being compressed, are relevant. Various motion detection sensors, such as tension sensors, resistive strain sensors, etc. allow tracking the mutual displacement between two points of the sample surface in accordance with the applied force. Optical methods in deformable solid mechanics are widely used to study mechanical properties of materials and during the strain-stress state analysis of the deformable elements of machines and structures, in the design and testing of constructions durability, non-destructive testing. Optical methods for displacements measurements have significant advantages: contact-free recording of displacements, non-destructive methods, elimination of the mechanical impact on the sample surface, a full measuring field, no dependence on the type of tested material whether it is metal or composite. In paper [10], we used one of the optical methods, the shadow moire method, to measure out-of-plane displacements in composites with artificially created delaminations under compressive loads. The moire fringe method provides a visual representation of the distribution of deformations but does not provide high measurement accuracy. It is only reasonable where relatively large deformations are expected to occur, tasks related to the analysis of plastically deformed media, or the behavior of structures under the creep conditions [11]. In paper [12], the authors measured the deformation of composite samples under post-impact compressive loads using the electronic speckle pattern interferometry. This method is not suitable for measuring out-of-plane displacements. Speckle pattern interferometry allows studying objects that are not available for direct observation to measure the microrelief, shape, and movement parameters [13].

One of the new and promising contact-free methods for strain-stress state analysis of materials is the digital image correlation (DIC) method, which is a contact-free optical method for registering movement and deformation fields on the surface of the object. In 1982, paper [14] by Peters W. H. and Ranson W. F. firstly mentioned the DIC method when measuring displacements and deformations, assuming that there is a one-to-one dependence between images before and after deformation.

Using the Vic-3D non-contact optical video system, a DIC-based mathematical apparatus, it becomes possible to solve the problems of strain measurement under the combined stress and fracture kinetics analysis in the process of cracks propagation during the compression of samples [15-21].

The main objectives of this study were to obtain new experimental data on changes in the residual strength of polymeric large-cell composite samples in post-impact compression tests with joint use of a system for registering deformation fields to analyze the kinetics of crack propagation on the surface of the samples.

MATERIAL SAMPLE

This research is concerned with CFRP plates used in the aviation industry with $[0/\pm45]_n$ layout sequence of 150 × 100 × 4 mm size based on VSE 1212 plastic binder (Fig. 1, a), as well as glass and carbon polymer panels with large-cell honeycomb (honey-cell) with cell thickness of 2 mm and a height of 10 mm (Fig. 1, b) of 150 × 100 mm size. Composites with such an internal structure are used in the sound-absorbing circuit of an aircraft engine. For greater efficiency of noise reduction, one of the sides is subjected to perforation (Fig. 1, c).

This paper uses the following designations hereinafter fiberglass sample panels without perforation (G), with perforation (GP); carbon fiber without perforation (C), with perforation (CP). The mechanical properties of CFRP and GFRP samples presented at Tab. 1.

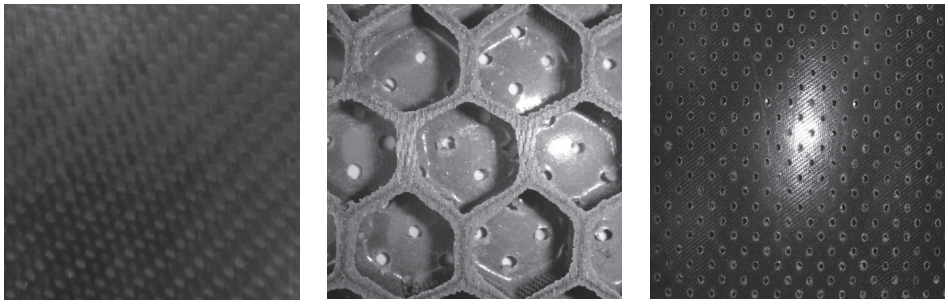

a *b* *c*

Figure 1: Photo of the CFRP sample (a), the internal large-cell honeycomb core of composite sample panels (b), the outer skin of the perforated sample (c).

Property	CFRP	GFRP	Unit
Tensile strength	850	420	MPa
Tensile modulus	67	27	GPa
Compressive strength	720	540	MPa
Sear strength	73	85	MPa
Flexural strength	1020	665	MPa

Table 1: The mechanical properties of CFRP and GFRP materials.

For honeycomb filler of sandwich panels, technical characteristics are shown in Tab. 2.

Property	CFRP/GFRP	Unit
Density	90-110	kg/m^3
Compressive strength	3.5-5.7	MPa
Operating temperature	160	°C

Table 2: The technical characteristics of honeycomb's cell.

The material was provided by an enterprise for the production of composite products for aviation and missile purposes as part of joint research work.

EQUIPMENT AND METHODS OF TESTING

This work was carried out in Perm National Research Polytechnic University using Unique Scientific Equipment «Complex of testing and diagnostic equipment for studying properties of structural and functional materials under complex thermomechanical loading».

The test methods, sample sizes, striker geometry, and test systems conformed to the recommendations of ASTM D7136, ASTM D7137 standards [22,23]. Testing was carried out on CFRP plates with a $[0/\pm45]_n$ layout sequence of 150 × 100 × 4 mm size with a transverse local drop weight impact. All samples were divided into groups of 6 samples for each impact energy level: 0-25 J in increments of 5 J, while the mass of the hammer remained constant 5.01 kg. Instron CEAST 9350 vertical-type drop weight apparatus coper was used to make impact damage on the surface of the test material samples. The impact was made on the geometric center of the samples with a 16-mm in diameter hemispherical tip (Fig. 2). The fixing conditions corresponded to the ASTM D 7136 standard [23]. The sample was mounted on a 300 × 300 mm slab with a 125 × 75 mm cutout and clamped using four rubber-tipped toggle clamps at the same distance to prevent the sample from moving during impact.

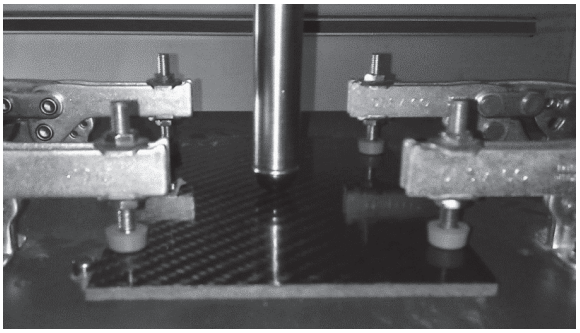

Figure 2: Photo of a carbon fiber sample under the falling-weight impact.

Quasi-static compression after impact (CAI) was performed on Instron 5982 electromechanical test system with the compression plate speed of V = 1.25 mm/min until complete destruction of or loss of stability by the sample. As an example, Fig. 3 shows a photo of a CFRP sample installed in a special compression fitting. Compression conditions after impact corresponded to the requirements of ASTM D 7137 [22].

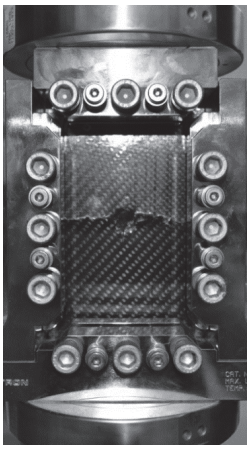

Figure 3: Photo of a carbon fiber sample installed in a compression fitting.

The test procedure consisted of 4 steps:

a. quasi-static compression of samples to evaluate the load-carrying capacity of P_{max} samples;
b. damage caused at the local, transverse to the sample plane, impact with the determination of the through and through penetration energy of the sample E_{max};
c. impact of different intensity $e'=\delta \cdot E_{max}$, where δ is [0;1];
d. quasi-static compression of the damaged samples with an estimated residual strength reduction P'.

Local out-of-plane impact followed by quasi-static compression of the composite sample plates is schematically shown in Fig. 4.

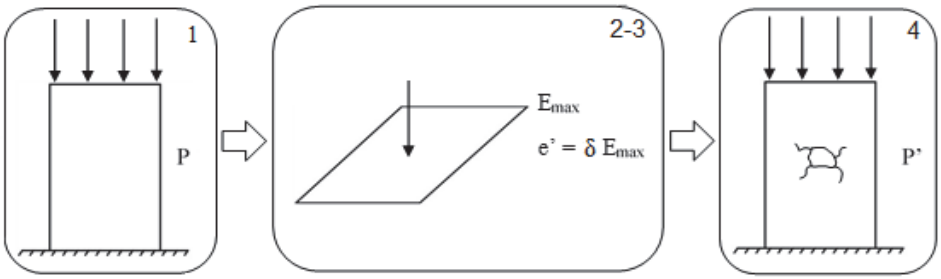

Figure 4: Schematic representation of impact and compression tests after impact.

Vic-3D (Correlated Solutions) three-dimensional digital optical system, whose mathematical apparatus is based on the DIC method, was used to analyze the displacement and deformation fields during the test. The system consists of two digital black-and-white 4-megapixel Q-400 cameras with XENOPLAN 28 mm f/2.0 lens, the shooting speed was 15 frames per second (fps). The images obtained during the experiment were processed using the DIC software. The processing parameters were as follows: the subset size was 43×43 pixels and the increment size (distance between subsets) was 5 pixels. The video system software provides for the use of different correlation criteria for the mathematical assessment of digital image compliance. This paper uses the normalized sum of squared difference NSSD criterion.

$$\chi_{NSSD} = \sum \left(\frac{\sum F_i G_i}{\sum G_i^2} G_i - F_i \right)^2 \quad (1)$$

where:
χ — images matching coefficient,
Fi — values of pixel intensity (brightness) levels for the first (reference) image,
Gi — values of pixel brightness levels for the second (subsequent) image.
This criterion is the least sensitive to changes in the illumination (brightness) of the sample during deformation [24].
For known displacement vectors of each point of the surface and its initial geometry, deformations can be calculated. They can be obtained directly by differentiating the neighbouring surface points displacement, or by analyzing the distortions of each neighbouring face used for correlation.
During post-processing by the Vic-3D system, deformation components were calculated using the finite strain tensor in Lagrange representation [24].

$$\varepsilon_{ij} = \frac{1}{2}\left(u_{i,j} + u_{j,i} + u_{k,i} u_{k,j} \right) \quad (2)$$

For the correct processing of experimental data, the data of the Vic-3D system software unit and the test machine controller were synchronized using the synchronization unit.
The accuracy of a non-contact optical system is influenced by the technical characteristics of lenses and digital cameras, namely the sensor sensitivity, resolution and possible shooting frequency. The accuracy of the obtained experimental data is also affected by the sample surface, setting and calibration of the chambers [24]. Based on the test results given in article [25], it was concluded that the use of the Vic-3D digital optical system allows determination of the deformation values on a fixed base, with an accuracy comparable to the data of the mounted longitudinal deformation sensor, the maximum possible deviation from the measured value of which is 0.15%.
Using the optical method of experimental mechanics: a highly effective digital image correlation method based on the Vic-3D non-contact three-dimensional digital optical system will allow for registering and analyzing the evolution of non-homogeneous displacement and deformation fields on the surface of structurally non-homogeneous material.

EVALUATION OF THE SURVIVABILITY OF CFRP PANELS IN CAI TESTS AT DIFFERENT ENERGY LEVELS

Following the results of the conducted series of tests, it was found that when impacts with energies less than 10 J, all samples were destroyed in the upper clamp area, which is not the preferred type of destruction (Fig. 5).
After the drop weight tests, a visual inspection of the samples was performed; all damages on the surface of the samples can be classified as follows (Fig. 6): a — no visible damage, b — visible cracks, c — significant damages in the form of cracks and dents (contact patch), d — reach-through breakdown.
Photos of the frontside and backside (reverse) surfaces of the samples are shown in Fig. 7.
As can be seen from the data obtained, for b-type damages (E = 5 J impact energy), cracks were observed on the frontside and backside of the sample without visible dents and bulges; for c-type (E = 10 J) — significant dents and cracks on the frontside, a bulge with bundles and local fiber breaks on the backside; for d-type (E = 25 J) — thorough damage along with the entire thickness of the sample.
Data on the material resistance to damage, permissible damages, and features of deformation and destruction of composites must be taken into account when designing high-duty units. The visual inspection, supported by the results of the residual strength assessment, greatly facilitates the monitoring of the structure survivability during its operation. For

analysing the changes in the residual load-bearing capacity of samples, the diagrams of the residual strength were built (Fig. 8). Each point on the diagram of residual strength is a separate test. Six samples were tested for each impact level. The results of statistical processing of the assessment of the residual strength of CFRP specimens are presented in Tab. 3.

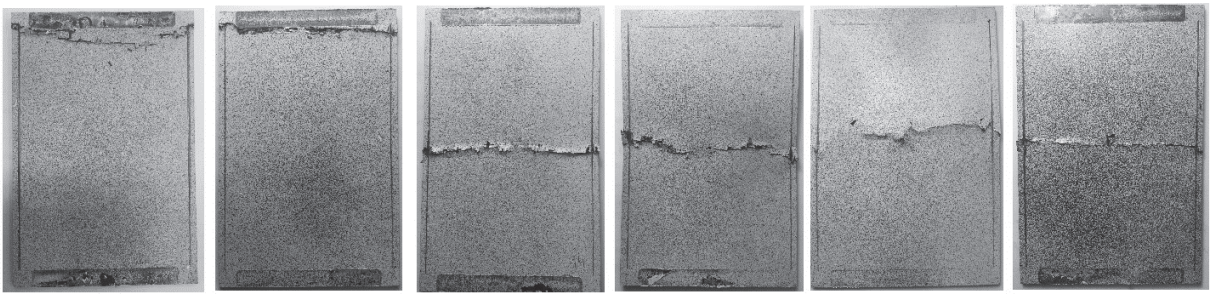

Figure 5: Characteristic types of destruction of CFRP samples in CAI tests.

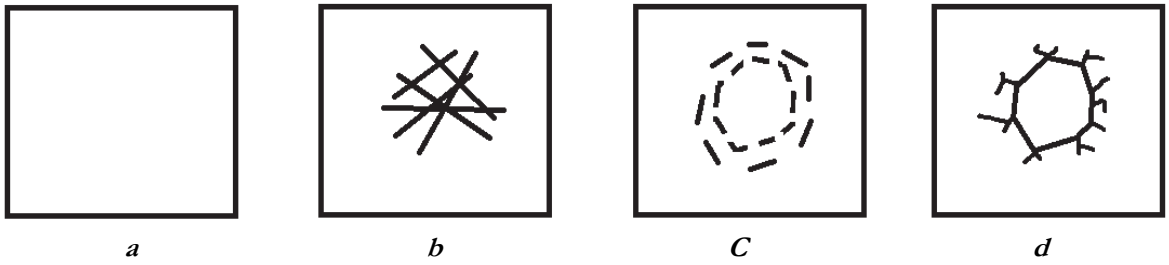

Figure 6: Post-impact damage types in samples scheme.

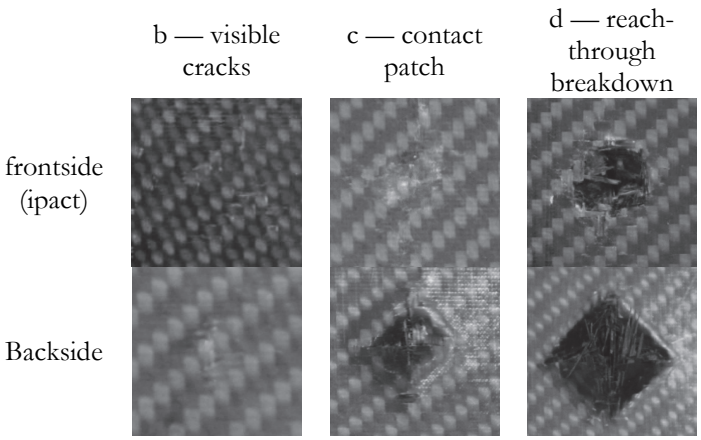

Figure 7: Photos of the sample surfaces.

The diagram (Fig. 8) for the residual strength shows a decrease in the level of strength characteristics by about 13% with a preliminary impact effect with 10 J energy. The destruction of the samples occurred in the area of the concentrators formed after the damages have been made, which indicates a sufficient degree of stress concentration. By increasing the impact energy up to 20 J, no significant decrease in strength properties was observed. For impact at 25 J energy, the maximum compression load was reduced by 33%. Therewith, the area in the impact range at energies of 5-10 J corresponds to the impactive sensitivity zone. The damages resulting from this impact energy can be visually undeterminable, and further operation of the structure will lead to reduced load-bearing capacity and destruction.

For a more detailed analysis of the process of samples destruction during compression, the Vic-3D non-contact optical video system was used. During compression at the initial moment, a local area of stretching strains ε_{yy} and ε_{xx}, surrounded

by an annular area of compression deformations, appears on the surface of the plate at the point of impact. Fig. 9 shows curves of the distribution of W out-of-plane horizontal displacement passing through the impact site on the sample. The results of W displacement on the z-axis are presented with 0.1 mm displacement for the ease of perception.

Energy of impact	<X>	S_{n-1}	CV
0	88.47	4.05	4.58
5	87.63	7.07	8.07
10	77.11	8.97	11.63
15	74.68	10.59	14.18
20	70.93	9.10	12.83
25	59.60	8.66	14.52

Table 3: The results of statistical processing of the assessment of the residual strength of CFRP specimens.

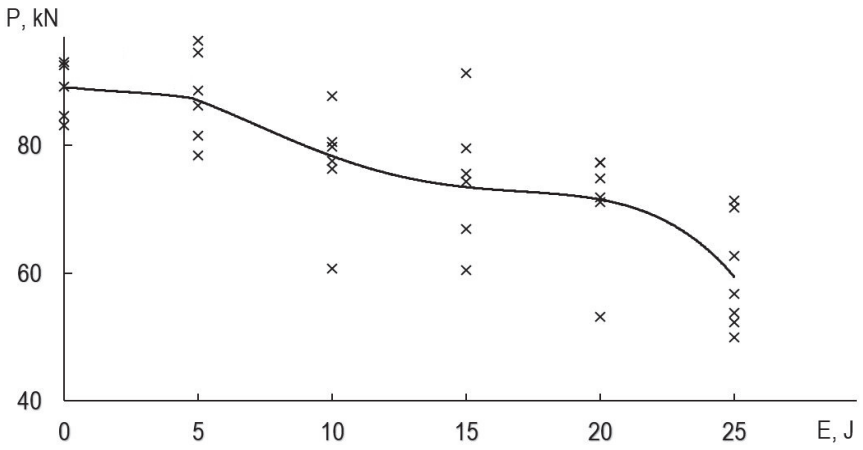

Figure 8: Residual strength diagram of CFRP samples.

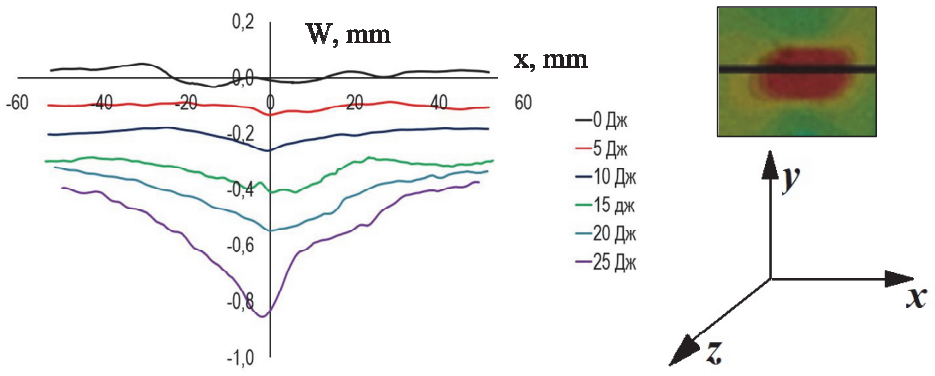

Figure 9: Profiles of out-of-plane displacement horizontal distribution on the surface of carbon fiber sample panels in post-impact compression tests.

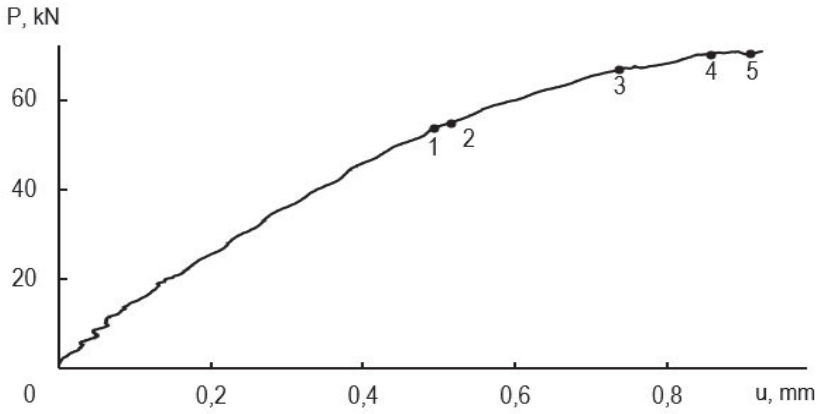

Figure 10: Loading diagram of a carbon fiber laminated sample in compression tests after 20 J impact energy.

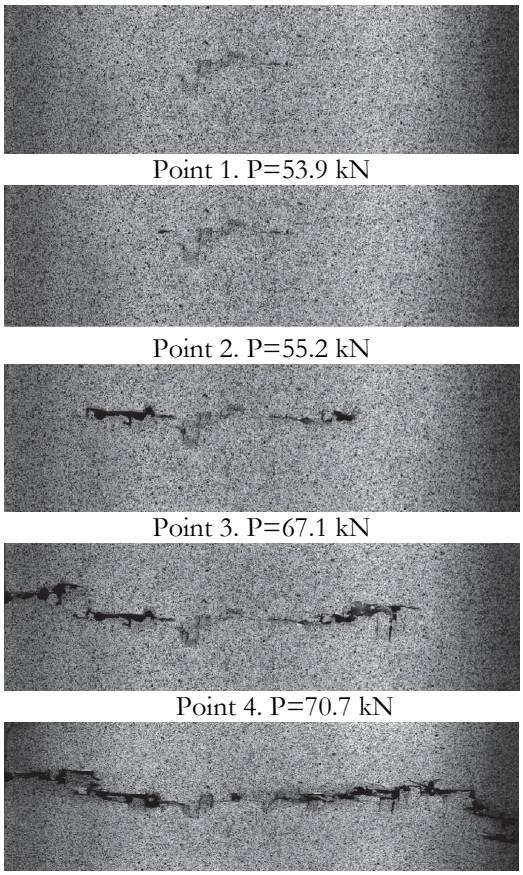

Point 1. P=53.9 kN

Point 2. P=55.2 kN

Point 3. P=67.1 kN

Point 4. P=70.7 kN

Point 5. P=70.2 kN

Figure 11: Photos of 20 J impact energy destruction (crack growth) area of the sample under the corresponding stress-strain conditions

Based on the results obtained, it can be noted that when the impact energy is 10 J or more, there is a local bulging in the damaged zone. At impact energies of 15, 20, and 25 J, local bulging is even greater because delamination is already spreading in this area and causes a significant reduction in the sample's stiffness. It can also be noted that as the compressive load increases, the deformation zone increases. According to the obtained profiles of out-of-plane displacement distribution, it can be judged at what impact energy the material was delaminated in the impact area. Delamination leads to bulging in the damaged area, as evidenced by the results (Fig. 9) obtained using the video system.
Following the result of the tests, deformation fields were built for each sample in its working area. During the analysis of deformation fields, it was revealed that at 5-10 J impact energy, the initial and final destruction of the sample occurs at the

impact site, without the development of a crack. As an example, the loading diagram (Fig. 10) shows points 1-6, for which non-homogeneous fields of deformation intensity ε_i are represented at the corresponding stress-strain conditions (Fig. 11) at 10 J impact energy. During loading, the central part of the sample contains the area with the maximum value of deformations, where subsequently localized deformation macro-fringes are formed and begin to grow (Fig. 11, points 1-3) having a direction at an angle of 45° to the side faces of the panel. With a further increase in the load, there is a further increase in deformation, the macro-fringes on the sample surface merge and form an area with a higher deformation value in the center (Fig. 11, points 4-6), while the upper and lower faces of the panel have deformation areas which are significantly less than in the center representing an impact site.

The image contrast has been adjusted to highlight rapid-growing surface cracks. At point 1, there is initial destruction, then there is a gradual development of cracks in the direction opposite to the compressive load application place to the edge of the panel on both sides of the impact site (Fig. 11, points 2-5). At high impact energies of 15-25 J, the most balanced crack development occurs than at low energies.

The use of the video system for registration of displacement and deformation fields during the compression tests after the impact of carbon fiber sample plates allowed to record and track the process of initiation and propagation of cracks caused by out-of-plane impact in the stress concentrators area. Tests with different levels of energy impact highlighted the impactive sensitivity threshold of the tested composite sample plates.

DEFORMATION AND DESTRUCTION OF LARGE-CELL COMPOSITE SAMPLE PANELS IN CAI TESTS

According to the previously developed method, a series of CAI tests were performed with different levels of impact: 1 J — minute damages, 5 J — cracks and dents on the outer skin of the sample, 10 J — significant damage to the outer skin, penetration of the surface layer, 50 J — a reach-through breakdown of the entire sample. Photos of sample surfaces are shown in Fig. 12. The types of damages received after the falling-weight impact tests were similar to the types described before in Fig. 6. When testing for impact with a falling weight, tracking of the contact patch, impact into the void or into the cell wall was not performed.

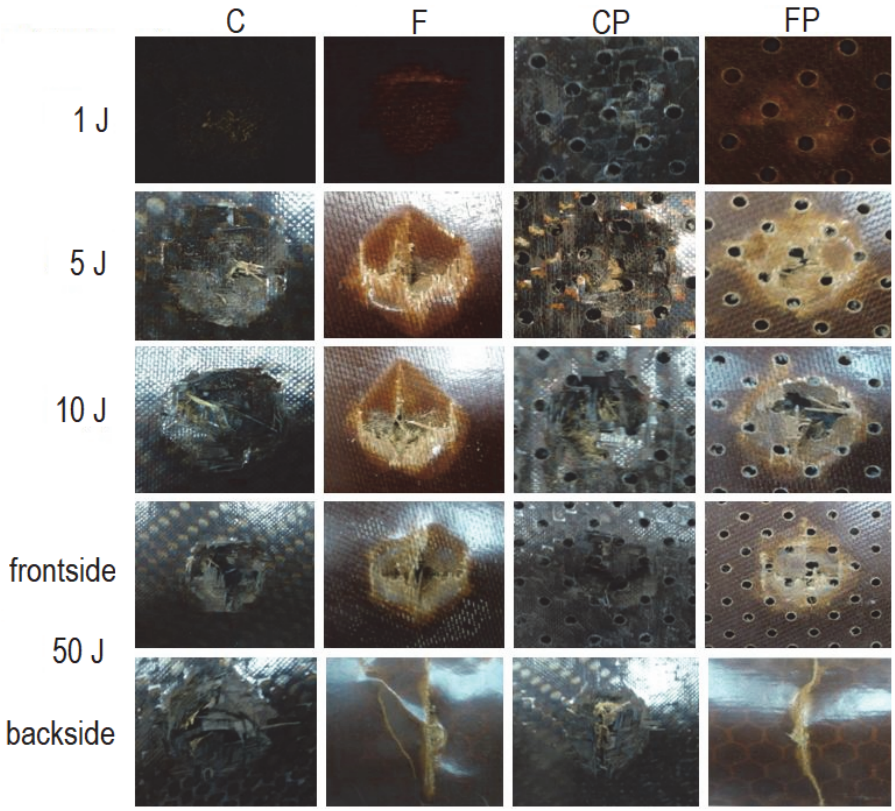

Figure 12: Photos of PCM samples after CAI tests.

The experimental data obtained reflecting the dependence of changes in the load-bearing capacity of the damaged large-cell polymeric sample panels are shown in the form of residual strength diagrams (Fig. 13).

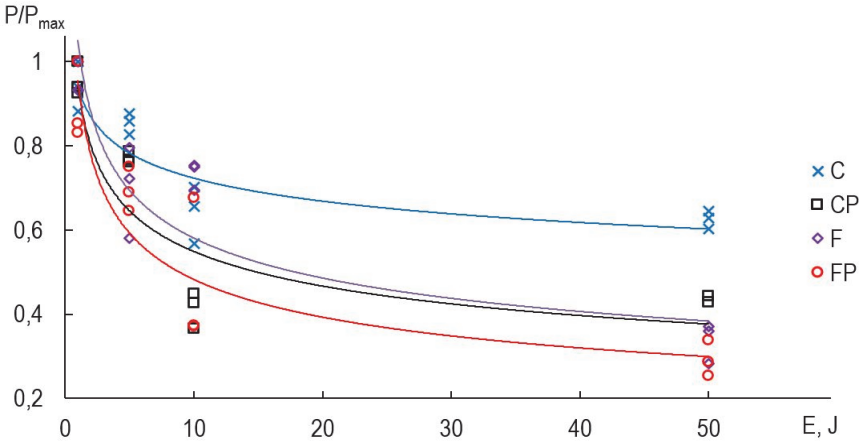

Figure 13: Diagram of the residual strength of composite large-cell sample panels.

It can be seen from the diagram that carbon fiber panel samples are more resistant during the local transverse impact. In the case of end-to-end damages, carbon fiber (C) honeycomb panels preserve their load-bearing capacity by 60%. For carbon fiber panels with perforation (CP) — 45%, fiberglass (F) — 35%, fiberglass with perforation (FP) — 30%, the 5 J energy impact resulted in a significant reduction in the residual load capacity, more than 15% compared to the nominal values. Photos of samples after CAI tests are shown in Fig. 14.
The results of statistical processing of test results for assessing residual strength are shown in Tab. 4.

Energy of impact	Sample	<X>	S_{n-1}	CV
1	CP	15.50	0.66	4.25
	FP	12.11	1.25	10.30
	C	16.48	1.04	6.33
	F	13.88	0.57	4.11
5	CP	12.52	0.21	1.71
	FP	9.41	0.71	7.52
	C	14.98	0.44	2.92
	F	10.17	1.60	15.70
10	CP	6.70	0.69	10.31
	FP	5.04	0.02	0.39
	C	11.25	1.19	10.60
	F	10.66	0.48	4.48
50	CP	7.08	0.17	2.36
	FP	3.97	0.58	14.64
	C	10.97	0.38	3.51
	F	4.91	0.70	14.36

Table 4: The results of statistical processing of test results for assessing residual strength of honey-comb samples.

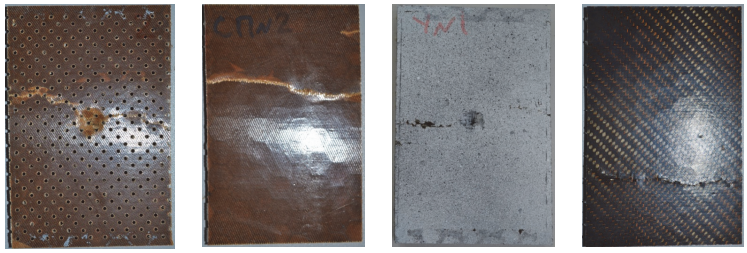

a *b*

Figure 14: Typical appearance of PCM sample panels after the compression testing (a – fiberglass, b – carbon) at impact energy of 10 J

Macrocracks that were formed during compression on the front (impact side) and back sides of the sample sprouted in different places, this type of propagation may be associated with the complex structure of the sample.
The presence of engineering concentrators (surface perforation) contributes to the unloading and dissipation of the destruction energy during the sample loading. Similar results were obtained by other researchers [26, 27].
Based on experimental data on the residual strength, further research was conducted for CFRP panels with and without perforation. For a more detailed analysis of the destruction mechanisms of the composite sample panels, the tests were performed using the Vic-3D video system for recording displacement and deformation fields.

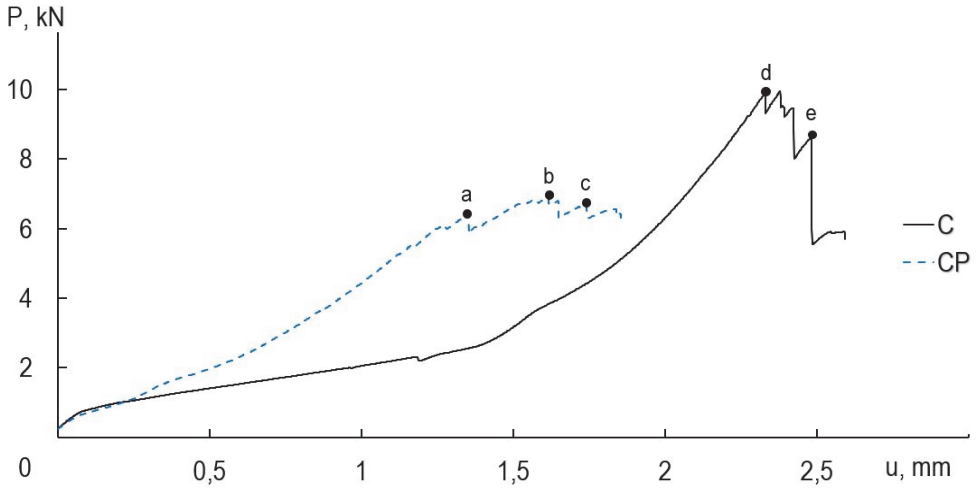

Figure 15: Diagram of loading the CFRP panels in CAI (10 J) tests.

The loading diagram of CFRP panels (Fig. 15) shows failures associated with structural destructions. The destruction occurred in several stages, each accompanied by a load drop of about 6%. With further loading, there was a slight increase in the load and further complete destruction of the sample. The drop-down section in the loading diagram for a CFRP specimen without perforation is the longest and averages 18% of the entire recorded diagram. For a perforated CFRP panel, there is practically no drop-off.
It is interesting to analyse the configuration of non-homogeneous deformation fields for carbon fiber panels. The loading diagram (Fig. 15) indicates points a-d, for which the deformation intensity fields ε_i are given for the corresponding stress-strain conditions (Fig. 16).
The given fields of deformation intensity at the maximum load clearly demonstrate the location of defects in turn leading to complete destruction of the sample. At points a and d, crack initiation is observed near the stress concentrator. At points b, c, e, the crack propagates further from the concentrator to the edge of the plate.
As a result of CAI tests of CFRP panels, deformation intensity fields were built. As an example, Fig. 17 shows the loading diagram and points a-f (at the maximum load value), for which the deformation intensity fields ε_i are given for the corresponding stress-strain conditions (Fig. 18).
Analyzing the loading diagrams (Fig. 17), it can be noted that the falling section in the loading diagram for fiberglass specimens both without perforation and with perforation at an impact energy of 50 J is longer than at an impact energy of 10 J. For fiberglass panels with and without perforation at impact energy 5 J, the falling section is practically absent. The resulting fields illustrate a high concentration of deformations on the left and right sides of the hole and a low

concentration on the upper and lower sides (the discharge area) in the direction of the load applied. If we compare the nature of destruction of fiberglass and carbon fiber sample panels, the damages have a similar topology. In the area of large deformations around the hole, there is a fiber break on both sides. Transverse cracks, where there is a concentration of deformation, spread across the width from the hole to the edge of the sample, across the load application site. The matrix transverse cracks were initiated in resin-rich channels. The transverse break caused further delamination, eventually resulting in the complete destruction of the sample.

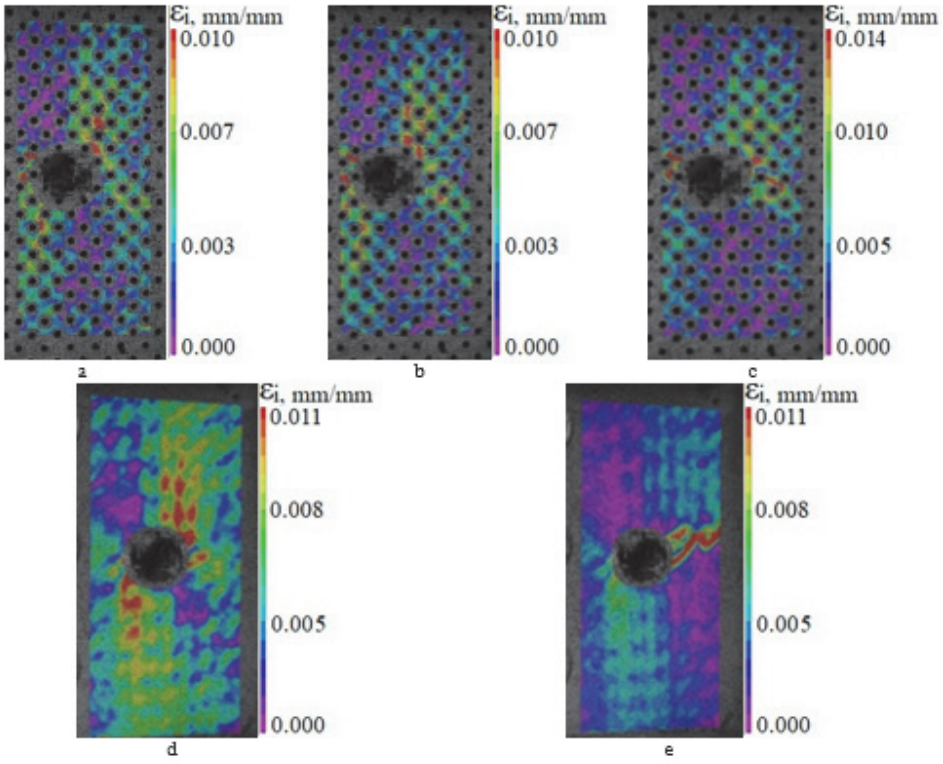

Figure 16: Deformation intensity fields ε_i of carbon fiber sample panels in compression tests after 10 J impact under the corresponding stress-strain conditions.

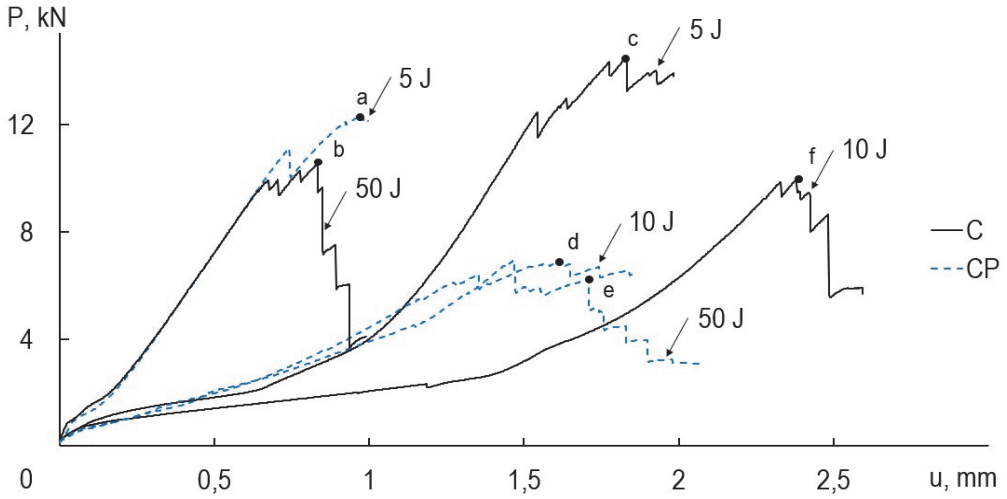

Figure 17: Loading diagram for CFRP panels in CAI tests at 5, 10 and 50 J.

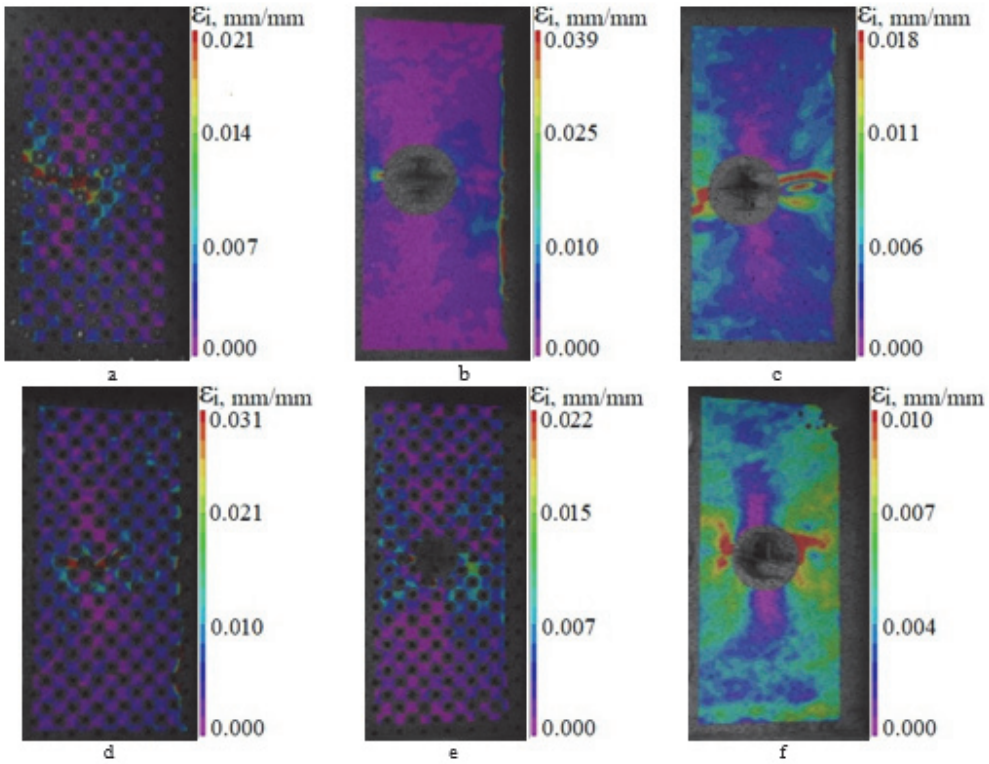

Figure 18: Deformation intensity fields ε_i of CFRP panels with and without perforation in compression tests after impact at 5, 10 and 50 J under the corresponding stress-strain conditions.

CONCLUSIONS

As a result of the conducted research, a method for evaluation of the residual strength of CFRP sandwich sample plates using a video system for analyzing the displacement and deformation fields was tested. A series of compression tests were performed after drop weight impact at different impact energies. Analysis of the results of mechanical tests allowed us to conclude there is an impactive sensitivity zone for the studied CFRP samples in the range of 5-10 J.

The use of the video system for registration of displacement and deformation fields during the compression tests after the impact of carbon fiber sample plates allowed to record and track the process of initiation and propagation of cracks caused by out-of-plane impact in the stress concentrators area. It is noted that the most equilibrium crack growth is observed in carbon fiber sample panels at the highest impact energies of 15-25 J. At the impact energy of 15, 20, and 25 J, local bulging occurs on the sample in the impact site, delamination is already spreading in this area and causes a significant decrease in the sample stiffness.

When testing GFRP and CFRP samples with and without perforation, it was found that CFRP panels had greater resistance (survivability) under the local transverse impact. In the case of end-to-end damages, carbon fiber (C) honeycomb panels preserve their load-bearing capacity by 60%. For carbon fiber panels with perforation (CP) — 45%, fiberglass (F) — 35%, fiberglass with perforation (FP) — 30%. We should also note that the impact with an energy of 5 J led to a significant reduction in the residual load-bearing capacity.

The nature of the deformation field distribution in fiberglass and carbon fiber large-cell sample panels is almost the same, as in panels with or without perforation. If we compare the nature of the destruction, the damages have similar topologies. According to the test findings, we should note that the destruction of samples began far from the site of damage. Thus, based on the data obtained using the Vic-3D non-contact three-dimensional digital optical system, we can arrive at the conclusion on the effectiveness of using this method to study the deformation patterns of composite sample panels.

ACKNOWLEDGEMENTS

The work is carrying out in Perm National Research Polytechnic University with financial support of grant of President of Russian Federation for government support of young Russian scientists (Grant No MK-1222.2020.8.).
The Experimental studies in the framework of the description of the mechanical behavior of structurally inhomogeneous materials were conducted within the State Assignment of the Ministry of Science and Higher Education of the Russian Federation (№ FSNM-2020-0027).

REFERENCES

[1] Erasov, V.S., Krylov, V.D., Panin, S.V., Goncharov, A.A. (2013). Tests of a polymer composite material for impact by a falling load, Aviation materials and technologies, 28(3), pp. 60-64.
[2] Kudrin, A.M., Karaeva, O.A., Gabriels, K.S., Solopchenko, A.V. (2018). Determination of the ultimate compressive strength of a polymer composite material after impact in accordance with ASTM D 7137, Bulletin of the Voronezh State Technical University, 14(2), pp. 164-169.
[3] Staroverov, O.A., Babushkin, A.V., Gorbunov, S.M. (2019). Evaluation of the damage degree to carbon-fiber composite materials under impact, PNRPU Mechanics Bulletin, 1, pp. 161-172. DOI: 10.15593/perm.mech/2019.1.14,
[4] Galehdaria, S.A., Kadkhodayana, M., Hadidi-Mouda, S. (2015). Analytical, experimental and numerical study of a graded honeycomb structure under in-plane impact load with low velocity, International Journal of Crashworthiness, 20, pp. 387-400. DOI: 10.1080/13588265.2015.1018739.
[5] Shahdin, A., Morlier, J., Michon, G., Mezeix, L., Bouvet, C., Gourinat, Y. (2011). Application of modal analysis for evaluation of the impact resistance of aerospace sandwich materials, Advanced aerospace applications. Conference proceedings of the society for experimental mechanics, 1(4), pp. 171-177. DOI 10.1007/978-1-4419-9302-1_15.
[6] Liang, S., Guillaumat, L., Gning, P.-B. (2015). Impact behaviour of flax/epoxy composite plates, International Journal of Impact Engineering, pp. 56-64. DOI; 10.1016/j.ijimpeng.2015.01.006.
[7] Lopresto, V., Langella, A., Papa, I. (2016). Residual Strength evaluation after impact tests in extreme conditions on CFRP laminates, Procedia Engineering, 167, pp. 138-142. DOI: 10.1016/j.proeng.2016.11.680.
[8] Wildemann, V.E., Staroverov, O.A., Tretyakov, M.P. (2020). Deformation and failure of polymer composite materials under preliminary cyclic and low-velocity impacts // IOP Conf. Series: Materials Science and Engineering, 747, 012034. DOI: 10.1088/1757-899X/747/1/012034.
[9] Wil'deman, V.E., Staroverov, O.A., Lobanov, D.S. (2018). Diagram and parameters of fatigue sensitivity for evaluating the residual strength of layered GFRP composites after preliminary cyclic loadings, Mechanics of Composite Materials, 54(3), pp. 313-320. DOI: 10.1007/s11029-018-9741-9.
[10] Suh, S.S., Han, N.L., Yang, J.M., Hahn, H.T. (2003). Compression behavior of stitched stiffened panel with a clearly visible stiffener impact damage, Composite Structures, 62(2), pp. 213–221. DOI: 10.1016/S0263-8223(03)00116-8.
[11] Sukharev, I.P., Ushakov, B.N. (1969). Investigations of deformations and stresses by the moire fringes method. Mechanical engineering. 208 p.
[12] Ruan, J., Wang, S., Tong, J., Shen, M., Aymerich, F., Priolo, P. (2012). Deformation measurement of composite laminate with impact damage under compressive loads, Polymers and Polymer Composites, 20(1-2), pp. 177–182. DOI: 10.1177/0967391112020001-234.
[13] Jones, R, Wykes, K. (1986). Golo graphic and speckle interferometry. - M.: Mir, 328 p.
[14] Peters, W. H., Ranson, W. F. (1982). Digital image techniques on experimental stress analysis, Optical Engineering, 21(3), pp. 427-431. DOI 10.1117/12.7972925.
[15] Yuan, Y., Wang, S. (2019). Measurement of the energy release rate of compressive failure in composites by combining infrared thermography and digital image correlation, Composites Part A: Applied Science and Manufacturing, 122, pp. 59-66. DOI: 10.1016/j.compositesa.2019.04.022.
[16] Liu, D., Bai, R., Lei, Z., Guo, J., Zou, J., Wu, W., Yan, C. (2020). Experimental and numerical study on compression-after-impact behavior of composite panels with foam-filled hat-stiffener, Ocean Engineering, 198, 106991. DOI: 10.1016/j.oceaneng.2020.106991.

[17] Tuo, H., Lu, Z., Ma, X., Xing, J., Zhang C. (2019). Damage and failure mechanism of thin composite laminates under low-velocity impact and compression-after-impact loading conditions, Composites Part B: Engineering, 163, pp. 642-654. DOI: 10.1016/j.compositesb.2019.01.006.
[18] Sun, X. C., Hallett, S. R. (2018). Failure mechanisms and damage evolution of laminated composites under compression after impact (CAI): Experimental and numerical study, Composites Part A: Applied Science and Manufacturing, 104, pp. 41-59. DOI: 10.1016/j.compositesa.2017.10.026.
[19] Tretyakova, T.V., Dushko, A.N., Strungar, E.M., Zubova, E.M., Lobanov, D.S. (2019). Comprehensive analysis of mechanical behavior and fracture processes of specimens of three-dimensional reinforced carbon fiber in tensile tests, PNRPU Mechanics Bulletin, 1, pp. 173-183. DOI: 10.15593/perm.mech/2019.1.15.
[20] Strungar, E. M., Wildemann, V. E. (2020). Inelastic deformation and destruction of fiber-laminated polymer composites in stress concentration zones, Frattura ed Integrità Strutturale, 53, pp. 406-416. DOI: 10.3221/IGF-ESIS.53.31.
[21] Strungar, E. M., Lobanov, D.S. (2020). Mathematical data processing according to digital image correlation method for polymer composites, Frattura ed Integrità Strutturale, 54, pp. 56-65. DOI: 10.3221/IGF-ESIS.54.04.
[22] ASTM D7137 / D7137M – 17. Standard Test Method for Compressive Residual Strength Properties of Damaged Polymer Matrix Composite Plates
[23] ASTM D7136/7136M – 15. Standard Test Method for Measuring the Damage Resistance of a Fiber-Reinforced Polymer Matrix Composite to a Drop-Weight Impact Event
[24] Sutton, M.A., Orteu, J.-J., Schreier,H. (2009). Image Correlation for Shape, Motion and Deformation Measurements. – University of South Carolina, Columbia, SC, USA, 364 p.
[25] Wildeman, V.E., Strungar, E.M., Lobanov ,D.S., Voronkov, A.A. (2018). Evaluation of the performance of fiber-optic sensors embedded in a composite material using data from a digital optical video deformation analysis system, Defektoskopiya, 1, pp. 65-71.
[26] Zhang, X., Xu, F., Zang, Y., Feng, W. (2020). Experimental and numerical investigation on damage behavior of honeycomb sandwich panel subjected to low-velocity impact, Composite Structures, 236, 111882.
[27] Dai, X., Yuan, T., Zu, Z., Ye, H., Cheng, X., Yang, F. (2020). Experimental investigation on the response and residual compressive property of honeycomb sandwich structures under single and repeated low velocity impacts // Materials Today Communications, 25, 101309